Electronic Supplementary Material (ESI) for Green Chemistry.

Supplementary Information:

Selective hydrogenation of compounds derived from 5-hydroxymethyl furfural over Ru, Pd, and Cu catalysts

Elise B. Gilcher[a,b], Hochan Chang[a], George W. Huber[a], and James A. Dumesic[a,b]*

[a]Department of Chemical and Biological Engineering, University of Wisconsin-Madison, Madison, WI, USA.

[b]DOE Great Lakes Bioenergy Research Center, University of Wisconsin-Madison, 1552 University Avenue, Madison, WI, USA.

*Corresponding author: James A. Dumesic (jdumesic@wisc.edu)

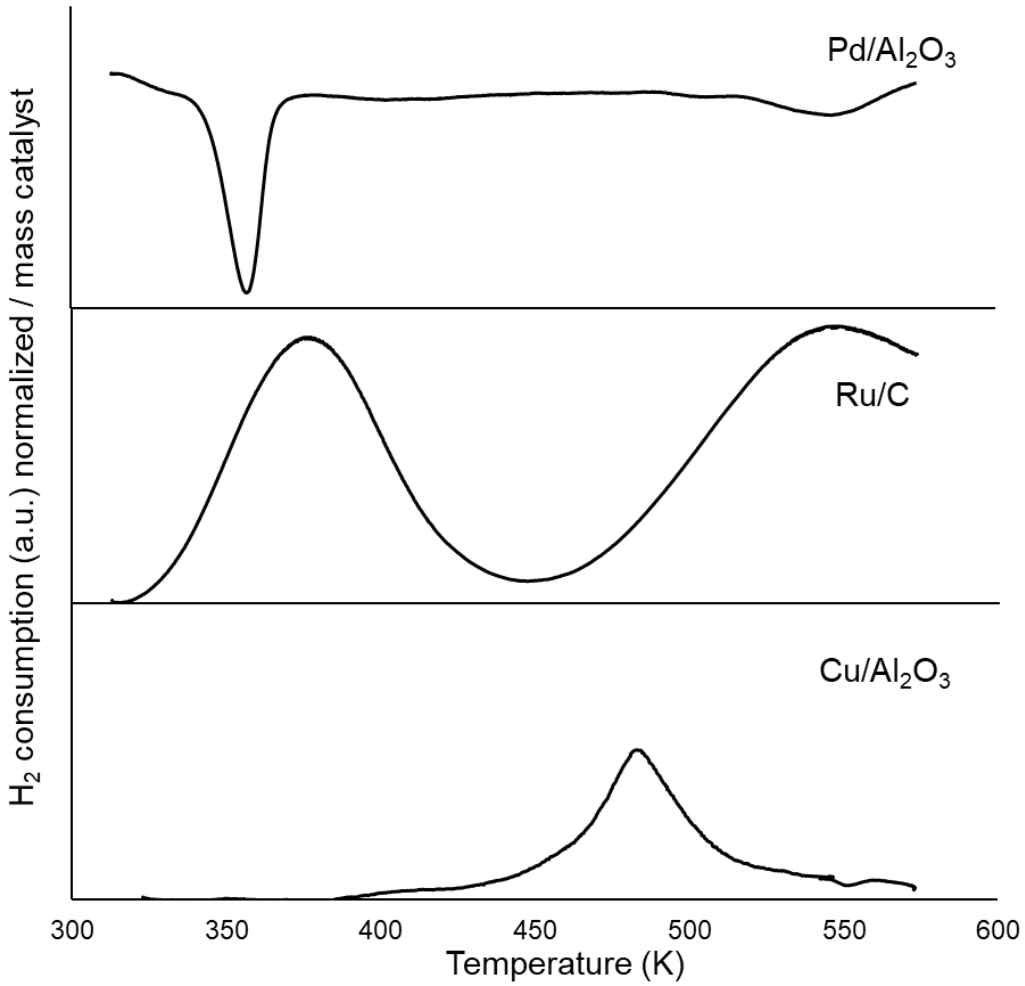

Figure S1. TPR profiles showing H_2 consumption as temperature is increased from 313 – 573 K over Pd/Al_2O_3 and Ru/C catalysts at a 10 K/min heating rate and from 323 – 573 K over Cu/Al_2O_3 at a 3 K/min heating. H_2 consumption is normalized per gram of catalyst.

Temperature programmed reduction (TPR) was performed on all catalysts to determine the degree of reduction at the reaction temperatures examined. Pd is known to readily dissociate H_2[1] and reduction can occur at room temperature. The Pd profile shows reduction of Pd/Al_2O_3 at low temperatures as expected, evidenced by the slight decrease in signal at low temperatures and the lack of significant positive consumption peaks. A sharp, negative peak is observed at 357 K and represents the release of hydrogen from the Pd surface. This peak aligns with literature reported temperatures for the decomposition of Pd-hydride species that form on Pd surfaces at room temperature.[2-3] As such, we anticipate that Pd(II) is completely reduced to Pd^0 at all temperatures examined in this work. The TPR profile for Ru/C showed large, broad features of H_2 consumption, with the first peak centered at 378 K and a second at 550 K. In the literature, Ru catalysts typically displays a peak representing H_2 consumption at 370 K.[4] However, a higher temperature consumption peak has been observed on the TPR spectra at roughly 450 K for Ru catalysts, and was attributed to more crystalline regions of the Ru oxides. **Figure S2** shows an additional, broad

peak centered at 800 K, which others in the literature have attributed to the partial gasification of the carbon support.[5-6] This characteristically broad peak partially overlaps the peak at 550 K. While the second peak observed in this spectrum is higher than those reported for crystalline RuO_2 structures in the literature, it is possible that this peak represents a similar, crystalline formation of RuO_2 on the Ru/C catalyst. Alternatively, this peak may be associated with the gasification of the carbon support. The reduction for this catalyst prior to reaction was at 523 K, which intersects the second Ru reduction peak. This reduction temperature allows us to examine the effect of a more metallic surface (Ru-523) versus a less reduced Ru surface (Ru-313). The Cu/Al_2O_3 catalyst showed a single, relatively small, peak at 490K, which agrees with similar TPR profiles from literature.[7-8] The reduction of Cu occurs well below the reduction temperature of 573 K prior to reaction in this work. Cu is therefore expected to be fully reduced at the treatment temperatures used.

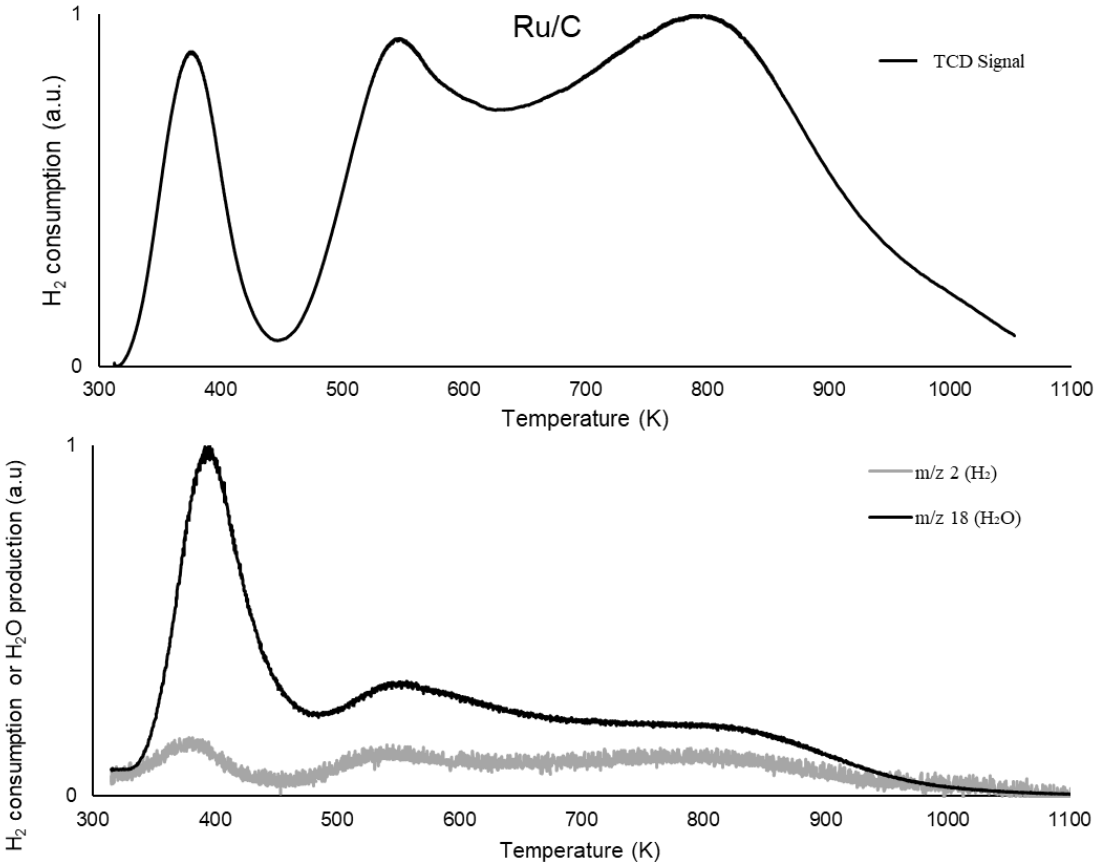

Figure S2. TPR profile over Ru/C showing H2 consumption as temperature is increased from 313 – 1073 K.

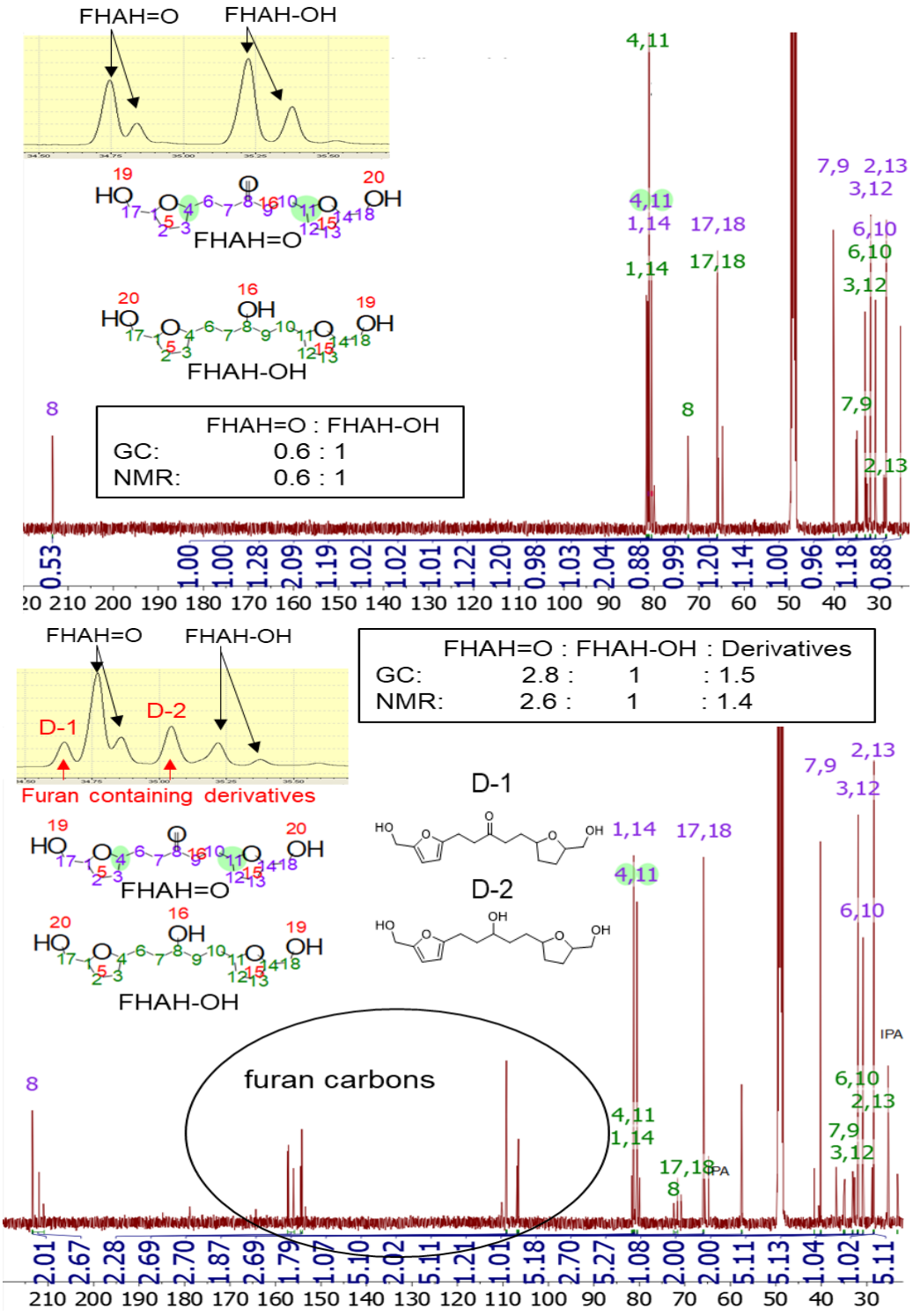

Figure S3. GC-FID profiles and quantitative ^{13}C NMR spectra of FHAH=O and FHAH-OH mixture compared to a mixture of FHAH=O, FHAH=O related derivatives, and FHAH-OH formed over Pd/Al_2O_3. Assignments are referenced from literature.[9] The mixture shows evidence of furan carbons, despite no presence of PHAH=O. A quantitative comparison of concentrations from the GC-FID and NMR analysis closely agree, showing that both derivative peaks contain carbons from furan rings. Potential structures of the derivative compounds are suggested.

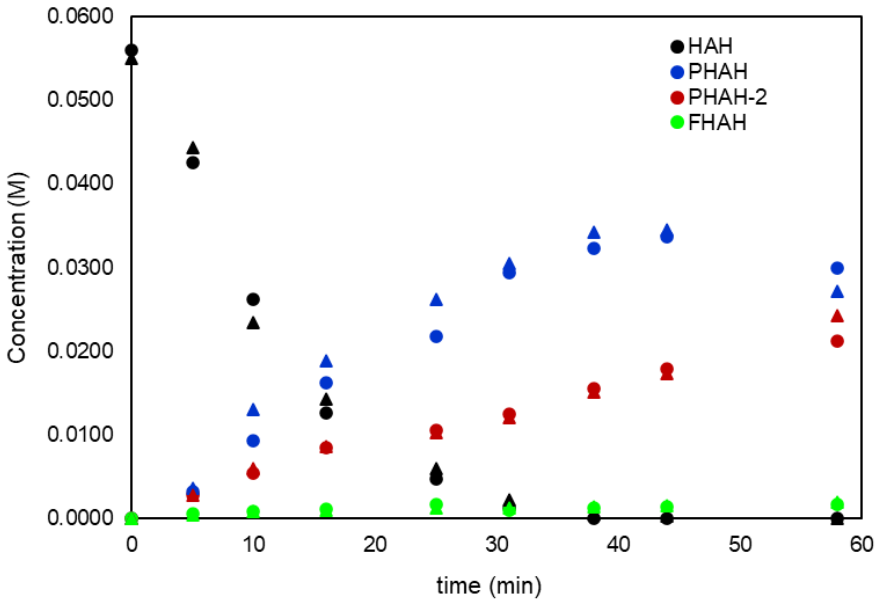

Figure S4. Overlay of two concentration profiles of 0.056 M HAH hydrogenation over 30 mg of unreduced 5 wt. % Ru/C at 333 K in IPA, loaded with 30 bar H_2. Circles and triangles represent multiple reaction runs at identical conditions, and errors are typically less than 0.003M for all species. (Black: HAH conversion, blue: PHAH=O conversion, red: FHAH=O conversion, green: FHAH-OH conversion).

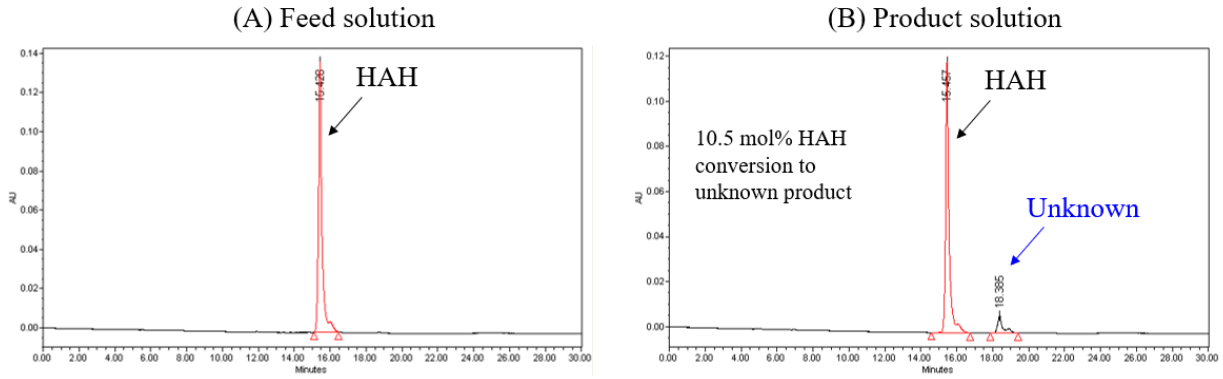

Figure S5. HPLC spectra showing (A) the HAH feed and (B) the product solution and degradation of HAH to an unknown product after 12 h control experiment without activate catalyst at 120 ˚C. Reaction conditions: 56 mM HAH in IPA with inert, unreduced catalyst (0.1 g of 3 wt% Cu/C, Aldrich), 120˚C, 35 bar H_2, 12 h reaction time.

A.

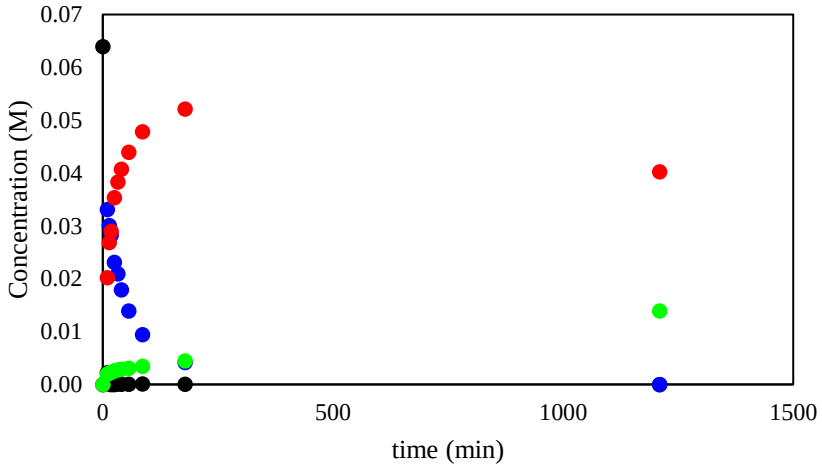

Figure S6. Concentration profile HAH and hydrogenation products over 30 mg Ru-523/C at 363 K. Ru-523/C was reduced at 523 K for 3 h under 58 bar H_2 prior to reaction. Reaction performed in batch; loaded with 460 mg HAH in 30 mL isopropyl alcohol and 30 bar H_2 (room temperature). Species identification identical to **Figure S4**.

Table S1. Comparison of 3 vs 5-step scheme fits for HAH hydrogenation over Pd/Al_2O_3, Ru-523/C, Ru-313/C, and Cu/Al_2O_3 using the Akaike Information Criterion (ΔAIC).

catalyst	T (K)	ΔAIC_C	
		3-step	5-step
Pd/Al_2O_3	313	10	0
	333	32	0
	363	70	0
	393	121	0
Ru-523/C	313	15	0
	333	40	0
	363	96	0
	393	130	0
Ru-313/C	313	26	0
	333	39	0
	363	98	0
	393	39	0
Cu/Al_2O_3	313	0	0
	333	0	4
	363	6	0
	393	9	0

The use of the Akaike Information Criterion (AIC) for kinetic model selection is described elsewhere in detail.[10] Briefly, the following equations were applied:

Eqn. 1: $AIC = N \ln\left(\frac{SS_E}{N}\right) + 2(K)$

where N is the number of observations (concentration datapoints), SS_E is the sum of the squares error, and K is the number of parameters (k_i). However, since the ratio of observations to parameters (N/k_i) is less than 40, a corrected AIC factor, AIC_C was used to account for the smaller sample size.[11]

Eqn. 2: $AIC_c = AIC + \frac{2K(K+1)}{N-K-1}$

Finally, the difference between the lowest AIC_C value and the highest value were shown as follows:

Eqn. 3: $\Delta AIC_i = AIC_i - \min(AIC_i)$

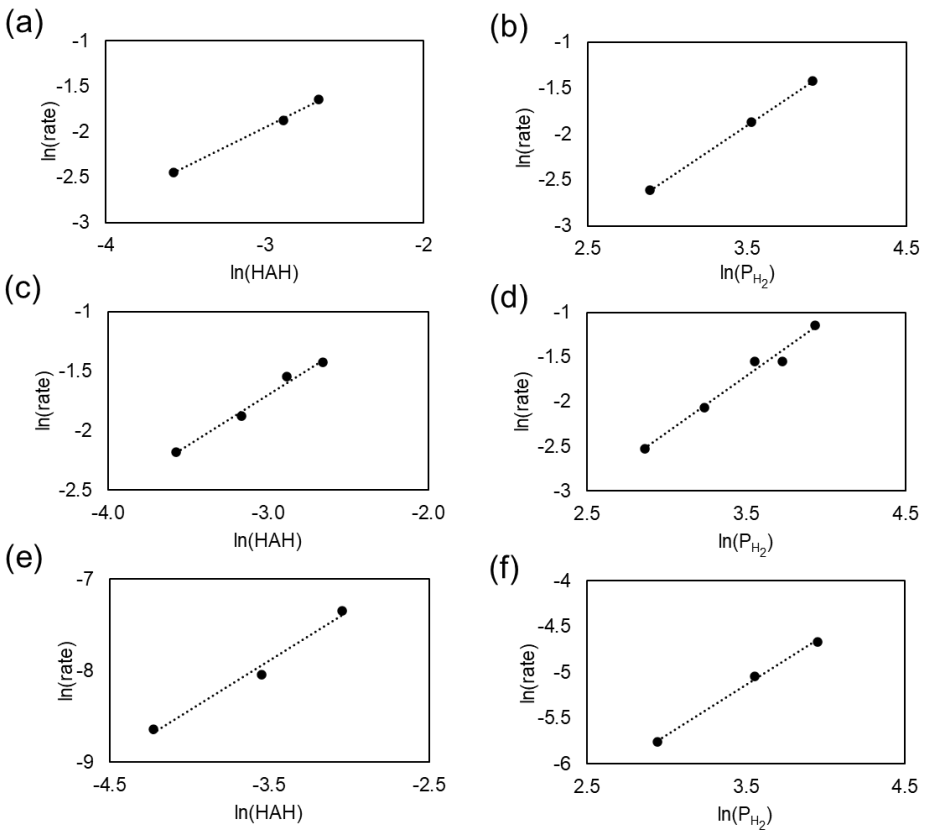

Figure S7. The effect of HAH concentration and hydrogen partial pressure on the rate of HAH hydrogenation over 5 wt.% Pd/Al_2O_3 (a - b), 5 wt.% Ru/C (c - d), and 3.6 wt.% $Cu/\gamma\text{-}Al_2O_3$ (e - f). HAH concentration varied from 0.028 M to 0.070 M and H_2 loading partial pressures varied from 15 to 45 bar. Other information: (a) slope = 0.86 , R^2 = 1.00, 15 mg Pd/Al_2O_3, 30 mL IPA, 333 K, (b) slope = 1.16, R^2 = 1.00, 15 mg Pd/Al_2O_3, 30 mL IPA, 333 K, (c) slope = 0.85, R^2 = 0.99, 30 mg Ru/C, 30 mL IPA, 333 K (d) slope = 1.26, R^2 = 0.98, 30 mg Ru/C, 30 mL IPA, 333 K (e) slope = 1.08, R^2 = 0.98, 0.056 M, 100 mg $Cu/\gamma\text{-}Al_2O_3$, 30 mL IPA, 363 K, (f) slope = 1.09, R^2 = 1.00, 100 mg $Cu/\gamma\text{-}Al_2O_3$, 30 mL IPA, 363 K.

Table S2. Model calculated rate constants at T_{ref} = 333 K for the 4-step pathway over Pd/Al_2O_3 (no pretreatment), 5-step reaction pathway over Ru-523/C (reduced at 523 K for 3 h) and Ru-313/C (no pretreatment), and a 3-step reaction pathway over $Cu/\gamma\text{-}Al_2O_3$ (reduced at 573 K for 5 h) catalysts.

Steps		Pd/Al_2O_3 k_i (L min^{-1} g^{-1})	Ru-523/C k_i (L min^{-1} g^{-1})	Ru-313/C k_i (L min^{-1} g^{-1})	$Cu/\gamma\text{-}Al_2O_3$ k_i (L min^{-1} g^{-1})
1a	HAH → I-HAH	0.0648 ± 0.0147	0.0074 ± 0.0018	0.0532 ± 0.0071	0.0012 ± 0.0002
1b	I-HAH → PHAH=O				0.0005 ± 0.0001
2	PHAH=O → FHAH=O	0.0211 ± 0.0085	0.0012 ± 0.0008	0.0083 ± 0.0022	--
3	FHAH=O → FHAH-OH	--	0.0001 ± 0.0002	0.0004 ± 0.0014	--
4	HAH → FHAH=O	0.1238 ± 0.0171	0.0056 ± 0.0016	0.0142 ± 0.0048	--
5	HAH → FHAH-OH	0.0177 ± 0.0055	0.0028 ± 0.0012	0.0038 ± 0.0048	--
6	PHAH=O →PHAH-OH	--	--	--	0.0001 ± 0.0000

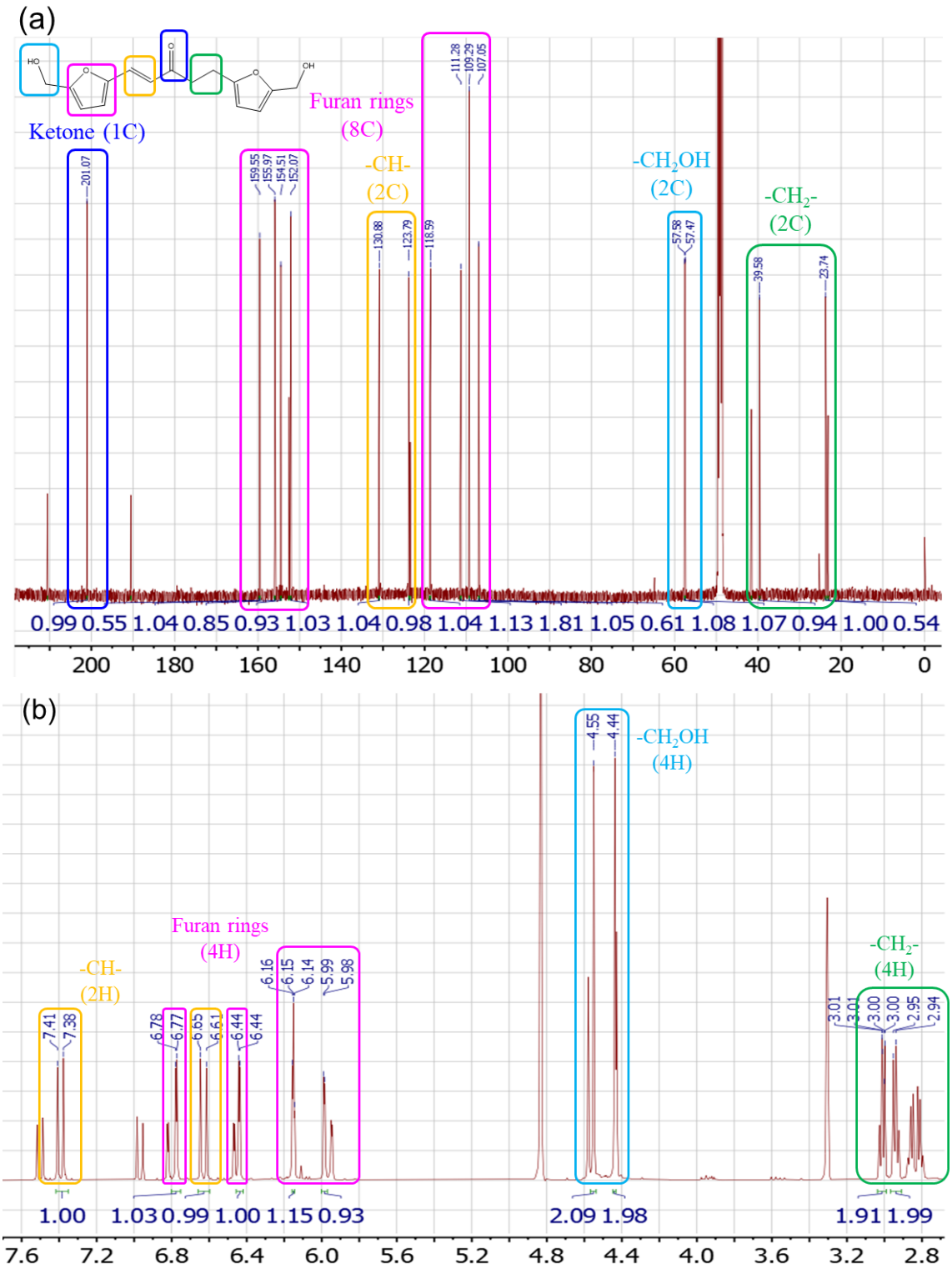

Figure S8. (a) ^{13}C quantitative NMR spectrum of 2:1 molar I-HAH and PHAH=O mixture (126 MHz, MeOD) I-HAH δ assignments: 201.07, 159.55, 155.97, 154.51, 152.07, 130.88, 123.79, 118.59, 111.28, 109.29, 107.05, 57.58, 57.47, 39.58, 23.74 ppm. (b) ^{1}H standard NMR spectrum of 2:1 molar I-HAH and PHAH=O mixture (500 MHz, MeOD) I-HAH δ assignments: 7.41, 7.38, 6.78, 6.77, 6.65, 6.61, 6.44, 6.43, 6.16, 6.14, 5.99, 5.98, 4.55, 4.44, 3.01-3.00, 2.95. 2.94 ppm.

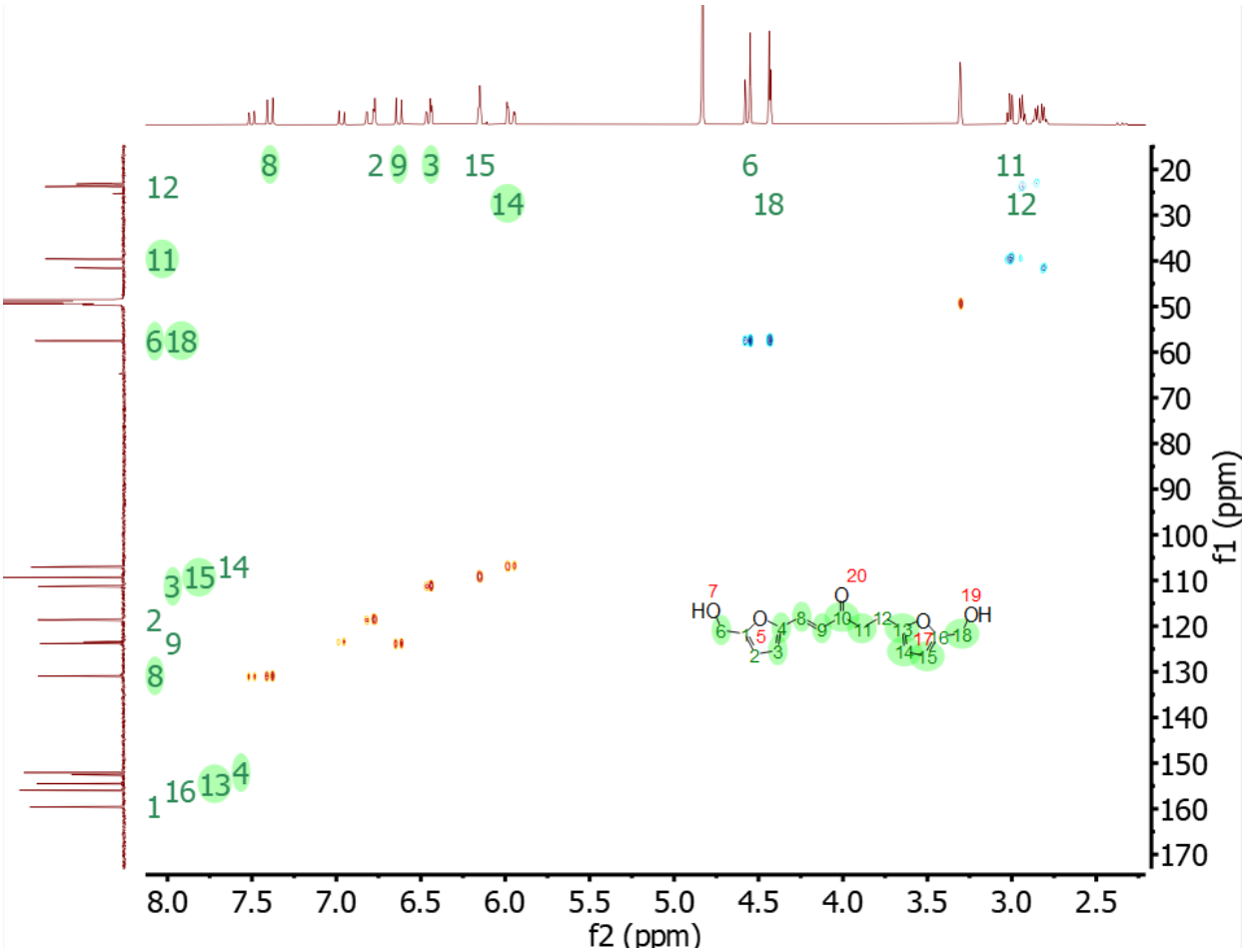

Figure S9. 2D HSQC NMR spectra of 2:1 molar I-HAH and PHAH=O mixture (126 MHz, MeOD, Blue: $=CH_2$, Red: $-CH_3$, $\equiv CH$).

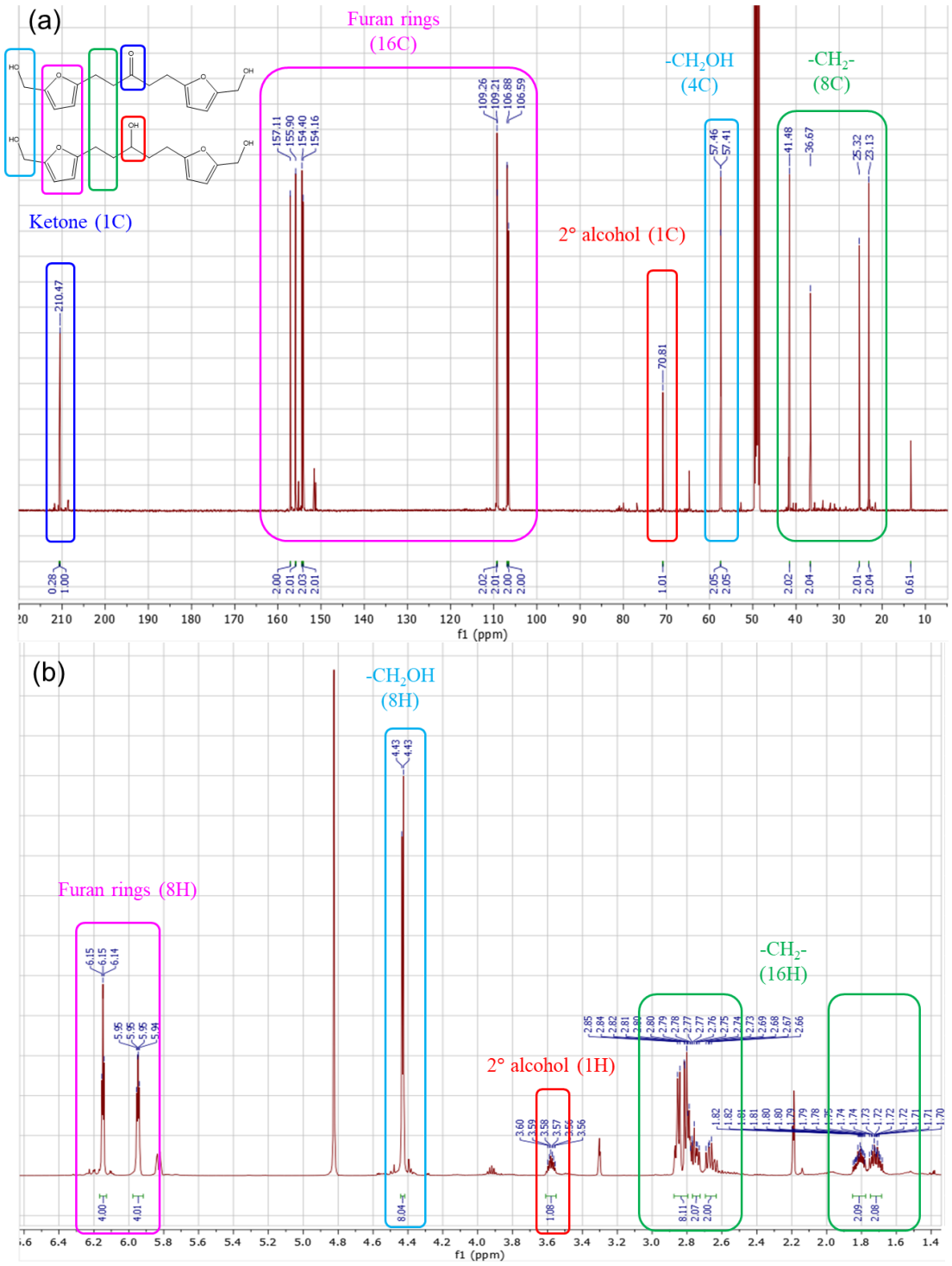

Figure S10. (a) ^{13}C quantitative NMR of PHAH=O and PHAH-OH mixture (126 MHz, MeOD) δ: 210.47, 157.11, 155.90, 154.40, 154.16, 109.26, 109.21, 106.88, 106.59, 70.81, 57.46, 57.41, 41.48, 36.67, 25.32, 23.13 ppm. (b) ^{1}H standard NMR spectrum of PHAH=O and PHAH-OH mixture (500 MHz, MeOD) δ: 6.15-6.14, 5.95-5.94, 4.43, 4.43, 3.60-3.56, 2.85-2.66, 1.82-1.78, 1.75-1.70 ppm.

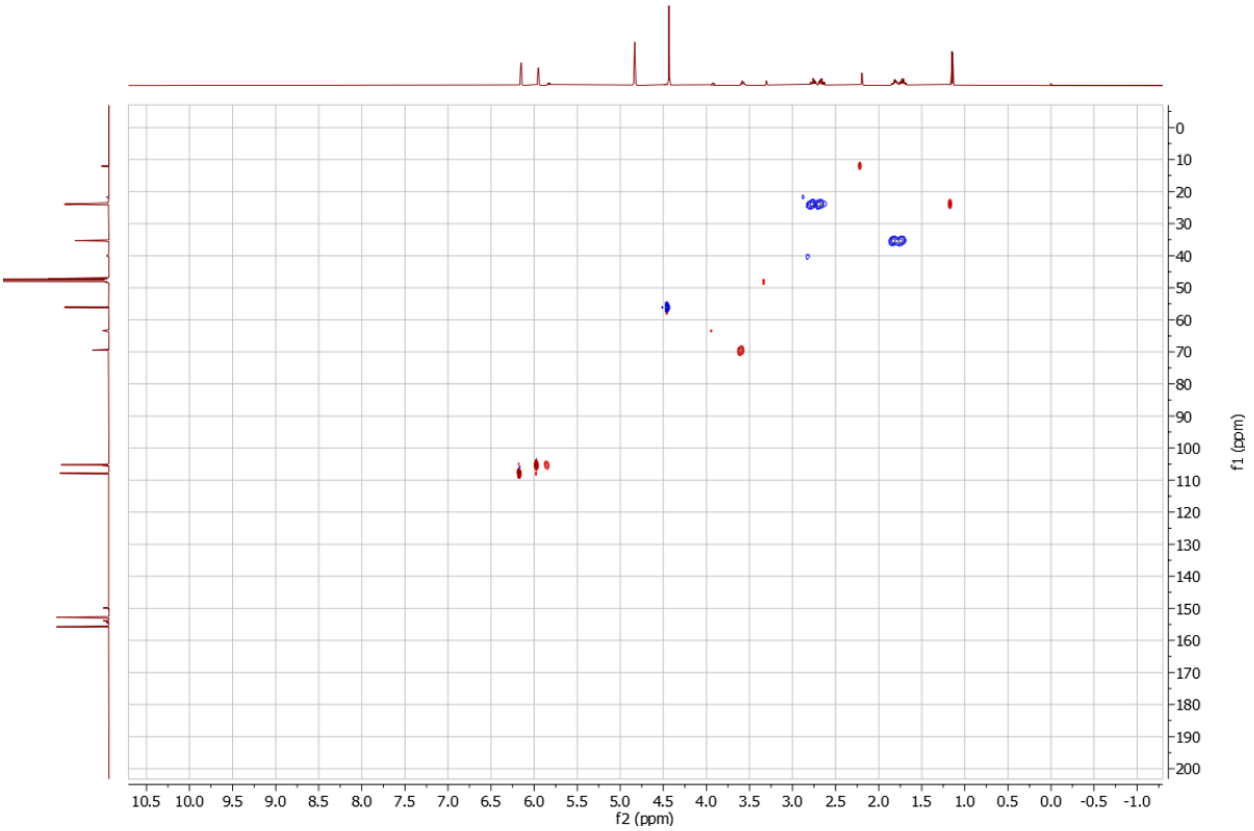

Figure S11. 2D HSQC NMR spectra of PHAH=O and PHAH-OH mixture (126 MHz, MeOD, Blue: $=CH_2$, Red: $-CH_3$, $\equiv CH$)

Pd/Al_2O_3

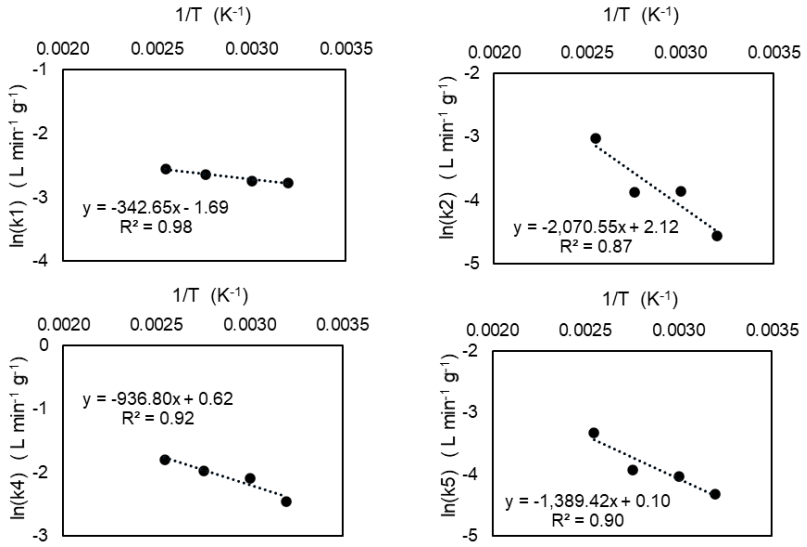

Figure S12. Arrhenius plots of HAH hydrogenation from kinetic model over Pd/Al_2O_3 for steps 1, 2, 4, and 5 in Scheme 2. T: 313 – 393 K, P: 30 bar H_2 loading at room temperature, C: 0.056 M HAH in 30 mL IPA, 20-30 mg Pd/Al_2O_3.

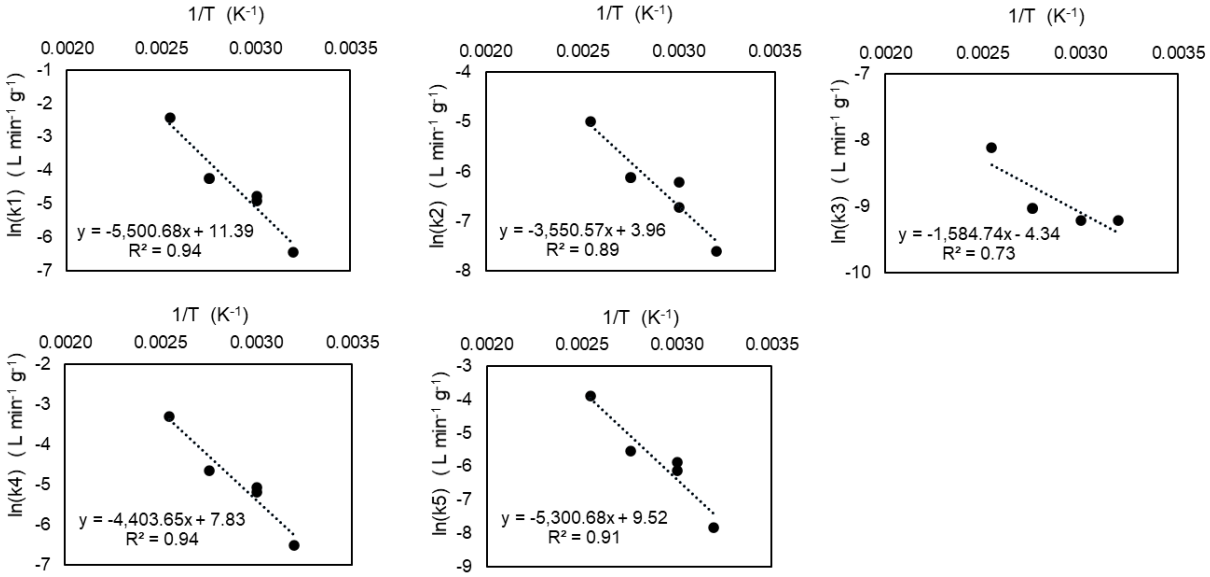

Figure S13. Arrhenius plots of HAH hydrogenation from kinetic model over Ru-523 /C for steps 1 - 5 in Scheme 2. Reduced Ru/C was treated at 523 K for 3 h under 58 bar H_2 prior to reaction. T: 313 – 393 K, P: 30 bar H_2 loading at room temperature, C: 0.056 M HAH in 30 mL IPA, 25-30 mg Ru/C.

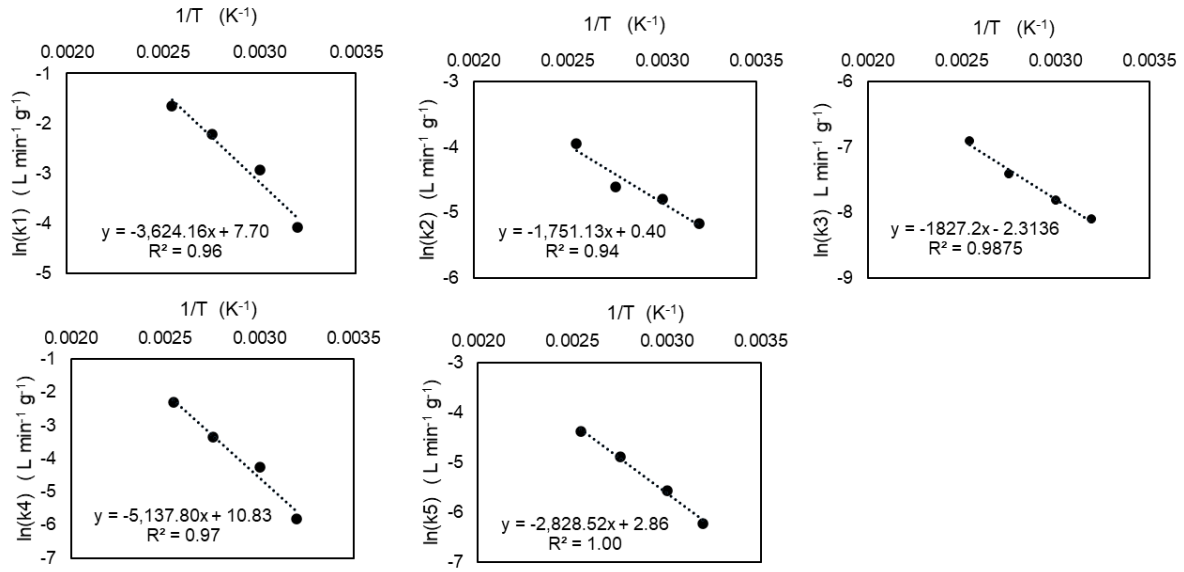

Figure S14. Arrhenius plots of HAH hydrogenation from kinetic model over Ru-313/C for steps 1 - 5 in Scheme 2. T: 313 – 393 K, P: 30 bar H_2 loading at room temperature, C: 0.056 M HAH in 30 mL IPA, 30-50 mg Ru/C.

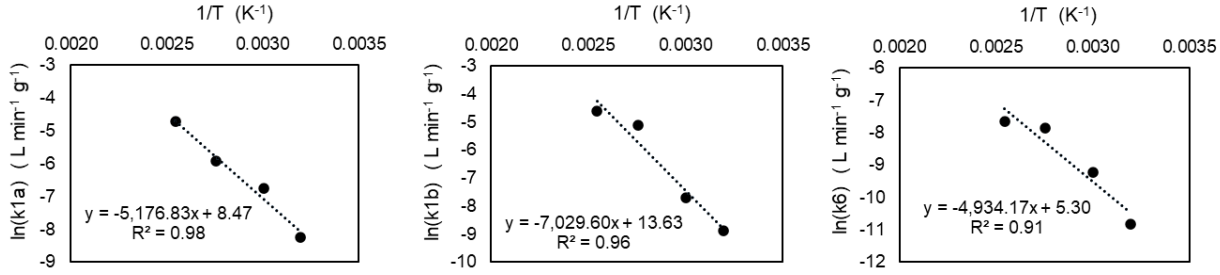

Figure S15. Arrhenius plots of HAH hydrogenation from kinetic model over Cu/Al_2O_3 for steps 1 - 3 in Scheme 3. Cu was reduced at 573 K for 5 h under 63 bar H_2 prior to reaction. T: 313 – 393 K, P: 30 bar loading at room temperature, C: 0.056 M HAH in 30 mL IPA, 100-150 mg Cu/Al_2O_3.

References

1. Luneau, M.; Lim, J. S.; Patel, D. A.; Sykes, E. C. H.; Friend, C. M.; Sautet, P., Guidelines to Achieving High Selectivity for the Hydrogenation of α, β-Unsaturated Aldehydes with Bimetallic and Dilute Alloy Catalysts: A Review. *Chemical Reviews* **2020,** *120* (23), 12834-12872.

2. Amorim, C.; Keane, M. A., Palladium supported on structured and nonstructured carbon: A consideration of Pd particle size and the nature of reactive hydrogen. *Journal of colloid and interface science* **2008,** *322* (1), 196-208.

3. Mironenko, R. M.; Belskaya, O. B.; Gulyaeva, T. I.; Nizovskii, A. I.; Kalinkin, A. V.; Bukhtiyarov, V. I.; Lavrenov, A. V.; Likholobov, V. A., Effect of the nature of carbon support on

the formation of active sites in Pd/C and Ru/C catalysts for hydrogenation of furfural. *Catalysis Today* **2015,** *249*, 145-152.
4. Huang, S.-Y.; Chang, S.-M.; Yeh, C.-t., Characterization of surface composition of platinum and ruthenium nanoalloys dispersed on active carbon. *The Journal of Physical Chemistry B* **2006,** *110* (1), 234-239.
5. Guerrero-Ruiz, A.; Sepuīlveda-Escribano, A.; Rodriīguez-Ramos, I., Carbon monoxide hydrogenation over carbon supported cobalt or ruthenium catalysts. Promoting effects of magnesium, vanadium and cerium oxides. *Applied Catalysis A: General* **1994,** *120* (1), 71-83.
6. Gallegos-Suarez, E.; Guerrero-Ruiz, A.; Rodríguez-Ramos, I.; Arcoya, A., Comparative study of the hydrogenolysis of glycerol over Ru-based catalysts supported on activated carbon, graphite, carbon nanotubes and KL-zeolite. *Chemical Engineering Journal* **2015,** *262*, 326-333.
7. Chen, C.-S.; Cheng, W.-H.; Lin, S.-S., Study of reverse water gas shift reaction by TPD, TPR and CO2 hydrogenation over potassium-promoted Cu/SiO2 catalyst. *Applied Catalysis A: General* **2003,** *238* (1), 55-67.
8. Bjelić, A.; Grilc, M.; Huš, M.; Likozar, B., Hydrogenation and hydrodeoxygenation of aromatic lignin monomers over Cu/C, Ni/C, Pd/C, Pt/C, Rh/C and Ru/C catalysts: mechanisms, reaction micro-kinetic modelling and quantitative structure-activity relationships. *Chemical Engineering Journal* **2019,** *359*, 305-320.
9. Chang, H.; Motagamwala, A. H.; Huber, G. W.; Dumesic, J. A., Synthesis of biomass-derived feedstocks for the polymers and fuels industries from 5-(hydroxymethyl) furfural (HMF) and acetone. *Green Chemistry* **2019,** *21* (20), 5532-5540.
10. Lindsay, M. J.; Walker, T. W.; Dumesic, J. A.; Rankin, S. A.; Huber, G. W., Production of monosaccharides and whey protein from acid whey waste streams in the dairy industry. *Green Chemistry* **2018,** *20* (8), 1824-1834.
11. Posada, D.; Buckley, T. R., Model selection and model averaging in phylogenetics: advantages of Akaike information criterion and Bayesian approaches over likelihood ratio tests. *Systematic biology* **2004,** *53* (5), 793-808.